JACS
JOURNAL OF THE AMERICAN CHEMICAL SOCIETY
Article
pubs.acs.org/JACS

Stabilizing Gold Adatoms by Thiophenyl Derivatives: A Possible Route toward Metal Redispersion

Bing Yang,[†] Yi Pan,[†] Xiao Lin,[†] Niklas Nilius,*[,†] Hans-Joachim Freund,[†] Catherine Hulot,[‡] Anne Giraud,[‡] Siegfried Blechert,*[,‡] Sergio Tosoni,[§] and Joachim Sauer*[,§]

[†]Fritz-Haber-Institut der MPG, Faradayweg 4-6, D-14195 Berlin, Germany

[‡]Institut für Chemie, Technische Universität Berlin, Straße des 17. Juni 135, D-10623 Berlin, Germany

[§]Institut für Chemie, Humboldt Universität zu Berlin, Brook-Taylor-Straße 2, D-12489 Berlin, Germany

Supporting Information

ABSTRACT: Tris(phenylthio)benzene molecules have been synthesized in order to explore their ability to trap single Au adatoms on an Au(111) surface. The resulting metal−organic complexes have been characterized with low-temperature scanning tunneling microscopy and infrared reflection absorption spectroscopy; possible structure models have been derived from density functional calculations. Upon room temperature deposition, the thiophenyl derivatives form dimer structures, comprising two molecules and six Au adatoms. Below 100 K, isolated molecules are found as well that have trapped up to six Au atoms. On the basis of the experimental results and calculated formation energies of the complexes, we discuss potential applications of the thioethers for the redispersion of metals on a catalyst surface. First experiments performed on Au particle ensembles prepared on alumina thin films suggest that the molecular ligands are indeed able to change the distribution of gold on the oxide surface.

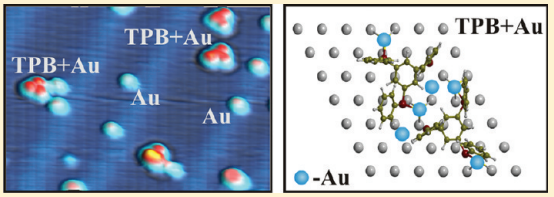

1. INTRODUCTION

The performance of supported metal catalysts is directly connected to the dispersion of the active metal species on the oxide surface.[1] The catalytic activity is found to scale with the inverse particle diameter, rendering smaller particles more reactive than their bulk-like counterparts.[2−5] One reason is the large fraction of under-coordinated, hence chemically active surface atoms in ultrasmall particles as well as their defect-rich or even amorphous structure. Also, the electronic properties of small aggregates are known to deviate from the respective bulk behavior,[6] and may be governed by charge transfer processes from the oxide support in addition.[7,8]

The particle-size distribution on supported metal catalysts is however not fixed during operation but subject to constant changes. The most relevant process is a diffusion-mediated (Ostwald) ripening, where small aggregates continuously lose atoms to larger ones.[9,10] Driving force for this material flow is the high surface-free-energy of the smallest metal deposits.[11] The ripening process gets enhanced by the elevated temperature and the interaction with gas-phase molecules during reaction conditions.[12] As a result, the particle-size distribution shifts toward larger values, a process that gives rise to a gradual deactivation of the catalyst. To keep the catalyst functional, the initial high dispersion of the metal needs therefore to be re-established by reversing the ripening process at a certain point.

Several proposals have been made in the literature, aiming at the redispersion of metal participles on oxide supports.[1] Most of them are based on the addition of halides, in particular of chlorine, to the catalyst feed-gas.[13−15] Although successful reactivation of the catalyst has been reported after such treatments, no atomic understanding of the associated processes could be achieved so far. In this study, we have explored an alternative approach to alter ripening processes at oxide surfaces. The concept relies on the stabilization of mobile surface species by means of strongly interacting ligand molecules. Those ligands need to be removed in a chemical or photochemical step later, which triggers the release of the trapped atoms and their recombination into small aggregates. Regular applications of the ligands might therefore maintain the high metal dispersion on the catalyst surface.

Given the tremendous interest in nanosized gold as catalytically active material,[2,3,5,16] we have developed and tested different thiophenyl derivatives, which are known to form strong Au−S bonds. We note, however, that our design concept can be extended to other catalytically relevant metals, such as Pt. We have investigated, from both experimental and theoretical points of view, the ability of the molecules to trap single Au atoms on an Au(111) surface. The binding configuration of the Au−ligand complexes was determined via low-temperature scanning tunneling microscopy (STM), while structure models were derived from density functional theory (DFT) calculations.[17] On the basis of computed Au−ligand binding energies, we discuss the ability of the ligands to stabilize metal adatoms on the surface and to break apart small gold clusters. We note that metal coordination by suitable

Received: January 11, 2012
Published: March 13, 2012

   dx.doi.org/10.1021/ja300304s | J. Am. Chem. Soc. 2012, 134, 11161−11167

molecular species has already been explored in great detail in order to produce metal−organic networks with potential applications in molecular electronics and surface patterning.[18−21]

In our approach, the ligand-mediated Au complexation involves the lattice-gas atoms that are intrinsically present on Au(111) at room temperature.[22] In order to mimic the real redispersion problem in catalysis, the single crystalline gold surface has been replaced with an ensemble of oxide-supported Au particles. Also in this case, the ligands are expected to stabilize single Au atoms, being exchanged among the deposits at elevated temperature. Indeed, new, ultrasmall Au aggregates were observed upon treating the particle ensemble with the thiophenyl derivatives at elevated pressure and temperature. We take this observation as first indication for the practicability of our redisperison approach.

2. EXPERIMENTS AND CALCULATIONS

The STM experiments have been carried out with a custom-built, ultra-high-vacuum instrument operated at 5 K.[23] The molecules were vapor-deposited from a Knudsen cell onto the sputtered/annealed Au(111) surface. To modify the density of mobile Au species on the surface, the sample temperature was varied between 100 and 300 K during exposure. Moreover, extra Au atoms were deposited from a hot tungsten filament onto the support. The development of Au−ligand adsorption complexes was deduced from constant-current STM images. The binding behavior of the molecules was further analyzed with infrared reflection absorption spectroscopy (IRAS) performed with an IFS 66 spectrometer from Bruker.

The DFT calculations were performed with the VASP code, using PBE as density functional.[24] The basis set has been defined with the projector-augmented-wave method using an energy cutoff of 300 eV.[25] Dispersion interactions were taken into account by a semiempirical C_6 term parametrized by Grimme and implemented for periodic boundary conditions (e.g., VASP) by Kerber.[26] The parameters for Au were adopted from a work of Tonigold and Gross.[27] We refer to this combined DFT/semiempirical approach as PBE+D (dispersion) and provide details in ref 17.

STM images were simulated with the Tersoff−Hamann model,[28] treating the tip as single s-orbital and assuming equal tunneling probability into all states inside a preselected energy window. This range was set from −0.3 eV to the Fermi level in agreement with the experimental conditions. Larger intervals did however not change the character of the images. The constant current mode was simulated by displaying a contrast map along a fixed electron-density isosurface.

3. RESULTS AND DISCUSSION

3.1. Synthesis of the Ligands and IR Fingerprint. The ligands used in this work are based on sulfur-containing aryl groups that can be tailor-made by changing the distance between the S centers and the electron densities at the molecular body. The interaction with gold is primarily governed by the formation of strong, covalent Au−S bonds, but further enhanced by the intermixing with the π-states of the aryls.[29,30] Main requirements for the synthesis were a high purity, a sufficient thermal stability and an adequate volatility of the ligands to enable direct sublimation into the gas phase. The first substance tested in this regard was 1,3,5-triazine that turned out to be unstable against desorption of the thiophenyl units. We then focused on different benzene derivatives, among which the 1,3,5-tris(phenylthio)benzene (TPB) was the most promising candidate. The molecule contains a central 1,3,5-tristhiobenzene unit and three outer phenyl rings attached via S atoms (Figure 1). It gains structural flexibility thanks to the peripheral rings that can easily rotate about their S−C axis. The

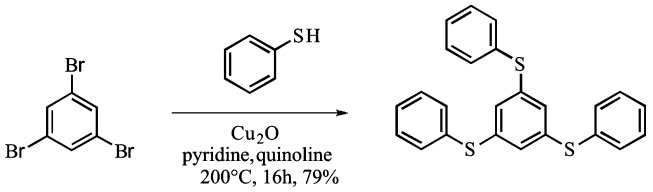

Figure 1. Synthesis of 1,3,5-tris(phenylthio)benzene via mixing tribromobenzene with thiophenol at 500 K for 16 h in the presence of Cu_2O. The final product concentration was as high as 79%.[31]

outer phenyls also impede strong intermolecular interactions, preferably without blocking the access of Au atoms to the molecular body. The ligands were synthesized using the Reifschneider method and purified with multiple chromatographic columns including preparative HPLC.[31] A second cleaning step was performed by outgassing the molecules at 350 K in vacuum.

The structural integrity of the ligands has been probed with IRAS performed in transmission and reflection geometry for TPB on glass and Au(111), respectively (Figure 2). The spectra

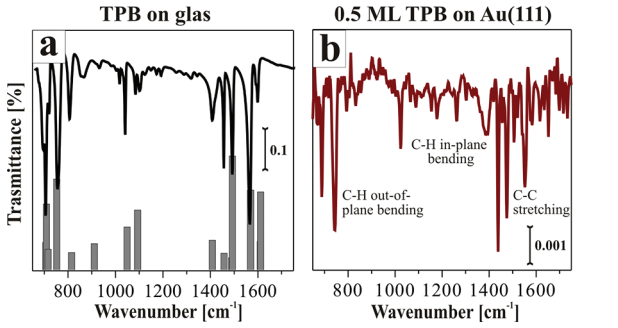

Figure 2. Infrared reflection−absorption spectra taken on (a) TPB on glass and (b) 0.5 ML TPB on Au(111). The bar graph in (a) visualizes the normal modes of the molecule, as determined with a Hessian harmonic frequency calculation at the DFT level.

exhibit an identical peak structure, suggesting the identity of the molecules on both substrates. Dissociation of the TPB on the Au(111) is therefore ruled out. The intensity variations of the IR bands are governed by the IRAS selection rules, which render only bands with large out-of-plane dipole components detectable on the gold surface. Moreover, the molecule has a defined binding geometry only at sub-monolayer coverage on Au(111), whereas thick TPB layers on glass are amorphous. The nature of the different IR bands has been elucidated with a normal-mode analysis performed on the DFT level (Figure 2a). Measured and calculated spectra are in reasonable agreement, which supports our conclusion that the TPB remains intact upon adsorption on the Au(111). Three absorption regions can be identified, as detailed in Table 1 of the Supporting Information. IR bands between 1500 and 1580 cm^{-1} are assigned to the C−C stretching modes of the phenyl rings.[32,33] The in-plane C−H bending motions of the phenyls give rise to absorption bands between 800 and 1450 cm^{-1}, while the out-of-plane C−H bending occurs in a frequency range from 680 to 750 cm^{-1}. Additional IR intensity at ∼3050 cm^{-1} reflects the C−H stretching motions of the rings (not shown). On the metal substrate, the bands are only detectable if the respective dipole moment has a substantial out-of-plane component. A detailed assignment of the IR bands to the different subunits of

dx.doi.org/10.1021/ja300304s | J. Am. Chem. Soc. 2012, 134, 11161−11167

the TPB and a correlation to the molecular binding geometry on the Au(111) can be found in the Supporting Information.

3.2. STM Fingerprints of TPB−Au Complexes on Au(111). Figure 3 shows three STM images of Au(111)

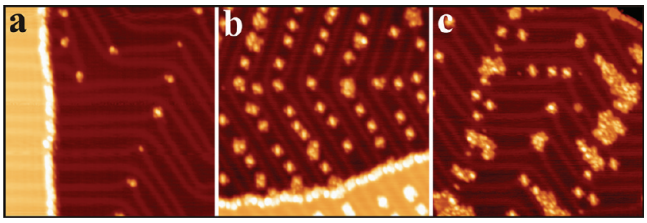

Figure 3. STM topographic images of Au(111) exposed to increasing amounts of TPB ligands at room temperature (450 × 450 Å^2, 0.3 V).

exposed to an increasing amount of TPB at room temperature. Individual ligand complexes are easily identified as protrusions that preferentially bind to the elbows of the Au(111) herringbone reconstruction and to the up-side of substrate step edges. With increasing coverage, the adsorbates also appear in the fcc domains of the herringbone reconstruction. In all cases, the individual entities remain well separated from each other, indicating a mainly repulsive interaction of TPB. Only at high and rapid exposure, the formation of irregularly shaped molecular islands is revealed on the Au(111) surface (Figure 3c).

Better-resolved STM images taken at low TPB exposure provide insight into the internal structure of the ligand complexes (Figure 4). The smallest unit that occurs only at

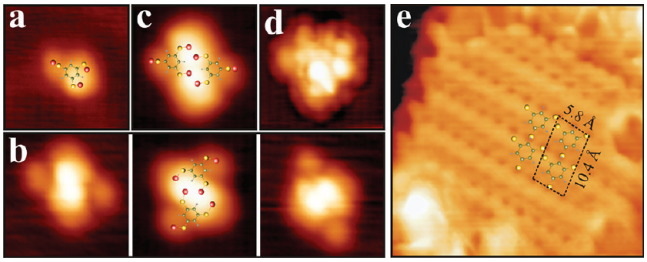

Figure 4. (a,d) STM images and superimposed structure models of different metal−organic complexes formed by TPB and Au adatoms at room temperature (30 × 30 Å^2, 0.5 V). The upright phenyl rings have been omitted in the models for the sake of clarity. (b) Short and (c) long dimer complex in different rotational configurations. (e) Molecular island formed upon rapid TPB dosing at 300 K (40 × 40 Å^2, 0.5 V). At this condition, the ligands are unable to trap enough Au atoms and aggregate into Au-free assemblies.

very low TPB coverage comprises a bright and a faint protrusion with 2.4 and 1.6 Å apparent height, respectively, separated by 7.5 Å (Figure 4a). The next bigger and by far more abundant complex is composed of two bright (2.6 Å height) and two dim protrusions (1.6 Å) in a cross-like configuration (Figure 4b,c). It seems to consist of two of the elementary building blocks described before and will therefore be referred to as a dimer in the following. Two isomers can be identified for the dimers that mainly differ in the spacing between the bright and dim maxima. In a short configuration, the bright protrusions are separated by 6−7 Å along an Au$\langle\bar{1}10\rangle$ direction, while the dim ones are spaced by almost 18 Å (Figure 4b). In a long configuration, the distance between the bright maxima increases to 8−9 Å, while the dim protrusions have a slightly smaller spacing of 16 Å (Figure 4c). The connecting axes between bright and dim maxima always enclose an angle of 80−90°. Due to the six-fold symmetry of the substrate, both isomers occur with three orientations rotated by 60° against each other, as shown for the short configuration in Figure 4b.

With increasing TPB exposure, irregular aggregates develop on the surface, being composed of the different building blocks discussed before (Figure 4d). A reliable structural analysis on the basis of the STM images is difficult in this case, because of the large variety of different configurations. Finally, flat molecular islands, characterized by a regular sequence of darker and brighter lines running along an Au $\langle\bar{1}10\rangle$ direction, develop at high and rapid TPB exposure (Figure 4e). The islands are composed of rhomboidal cells with 5.8 and 10.4 Å edge length and an enclosing angle of 75°. Its crystallographic relationship with the Au(111) lattice is described by a $\begin{pmatrix} 2 & 0 \\ 1 & 4 \end{pmatrix}$ matrix. The cell would be large enough to accommodate two TPB molecules in a slightly skewed configuration, in which two S atoms of each TPB give rise to the tiny depressions in the STM micrographs, while the third one is invisible due to a slight upward tilt of the central benzene ring (see sketch in Figure 4e). We note that this structure model is only tentative and cannot be confirmed in the context of this paper. All complexes described so far form spontaneously on the Au(111) upon TPB deposition at 300 K.

A second set of ad-structures can be produced by co-depositing small numbers of Au atoms onto a TPB-covered surface at 5 K, followed by gentle annealing to 100 K to promote diffusion. During heating, the adatoms disappear from the surface, as they attach either to the Au step edges or to the TPB ligands. The occurrence of new ad-features in the STM images suggests the second mechanism to be active. Some examples of those low-temperature complexes are displayed in Figure 5. They have a maximum diameter of 10−12 Å and are

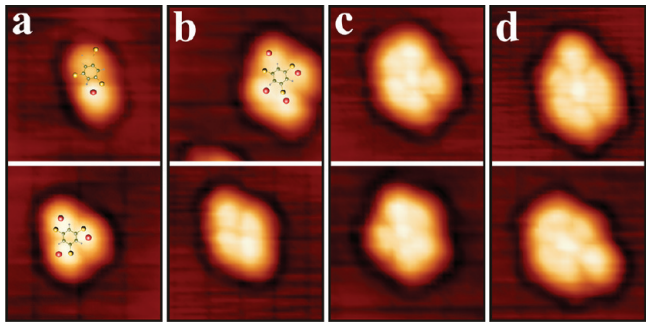

Figure 5. STM images and superimposed structure models for different metal−organic complexes, prepared by dosing Au atoms onto a TPB-covered gold surface below 100 K (30 × 30 Å^2, 0.5 V). The maxima in the images reflect the positions on the trapped Au atoms.

typically 1.5 Å high. This size is compatible with a single TPB molecule, which is why we refer to them as monomers in the following. The different ad-features can be classified by the number of lobes that surround the center protrusion. While structures with two and three lobes are displayed in image a, their number increases to four, five and six in images b−d. Apparently, the Au atoms dosed onto the surface are able to bind to the ligands in various configurations, all of them being stable only below room temperature.

dx.doi.org/10.1021/ja300304s | J. Am. Chem. Soc. 2012, 134, 11161−11167

A first model for the binding of the TPB molecules to the Au(111) may be obtained directly from the experiment. Not even the smallest, room-temperature units as shown in Figure 4a can be assigned to a single molecule, as they do not display the three-fold symmetry of TPB. This becomes even clearer for the dimer complexes in Figure 4b–d, which clearly exhibit a two-fold symmetry in the STM. Moreover, the co-adsorption experiments indicate that single Au atoms can be attached to the ligands, a process that was in fact envisioned when designing the molecules. The process of metal coordination would be possible even without dosing extra adatoms, as a dense lattice gas originating from the steady detachment of Au atoms from the surface steps is inherently present on the Au(111). The STM data therefore suggest the formation of metal–organic complexes by attaching mobile Au atoms to the TPB ligands. Even the number of adatoms per complex can be determined experimentally. With a 5 V bias pulse, a TPB dimer can be compartmentalized into six elementary constituents, all of them having the size of a single Au atom (Figure 6a,b). This

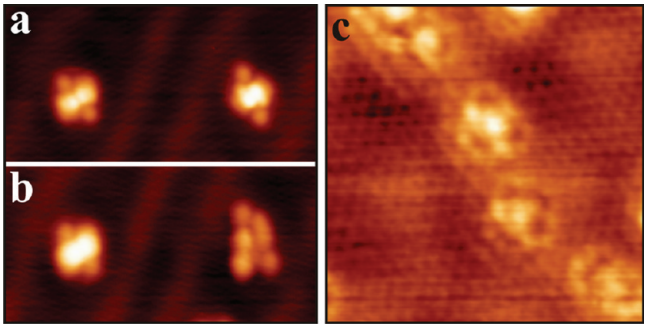

Figure 6. (a,b) TPB dimer structures on Au(111) before and after applying a +5 V pulse to the right entity (140 × 70 Å^2, −0.5 V). The species appearing after manipulation are the Au atoms that had been incorporated in the complex before. (c) TPB molecules deposited onto a bilayer FeO film grown on Pt(111) (60 × 60 Å^2, −0.8 V). As no Au-mediated adsorption scheme is available in this case, the three-fold symmetry of the TPB becomes visible.

manipulation experiment therefore indicates the number of incorporated Au atoms in the dimer to be six. Further evidence for the TPB–Au complexation reaction on Au(111) comes from a control experiment, where the ligands have been dosed onto an FeO thin film grown on Pt(111) (Figure 6c).[34] Evidently, this surface contains neither Au nor other metal adatoms that might interact with the ligand molecules. Indeed, the expected three-fold symmetry of isolated TPB species becomes immediately visible in this case and cross-shaped or multilobed features, being typical for Au(111), are absent. Moreover, the apparent height of the adsorbates has decreased from 2.6 Å on the Au(111) to 0.5 Å on the FeO/Pt surface. This height reduction is incompatible with the presence of metal atoms inside the ad-features and suggests that only the molecular electronic states governed by the large HOMO–LUMO gap are responsible for the image contrast on the oxide. The different appearance of TPB molecules on oxide and metal surfaces therefore supports our idea that metal–organic complexes develop on the Au(111) via TPB–Au complexation.

3.3. Theoretical Characterization of TPB–Au Complexes on Au(111). To confirm the binding model derived from the STM, we have performed an extensive computational search for thermodynamically stable TPB–Au complexes.[17] A natural starting point is a TPB molecule that lies flat on the gold surface and has a number of Au atoms attached. When optimizing this starting geometry, the central benzene ring remains flat with an interface distance of about 2 Å, while the peripheral rings turn upright (Figure 7). The central ring is

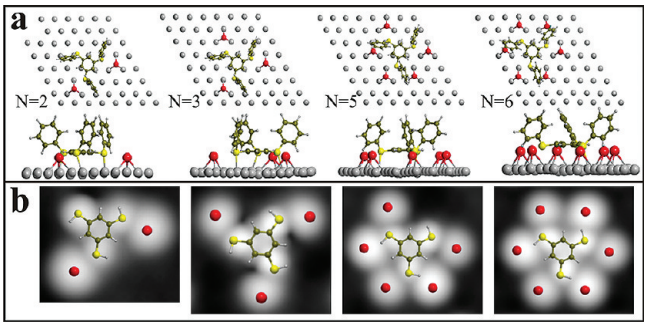

Figure 7. (a) Optimized structure from PBE+D calculations of a single TPB molecule on Au(111) after attaching two, three, five, and six Au adatoms (top and side view). (b) Simulated STM images with the ball models overlaid. The upright phenyl rings have been replaced with hydrogen atoms in this case. The images were obtained at an isodensity level of 0.001 |e|/Å^3. The resulting configurations correspond to the low-temperature monomer complexes observed in the experiment.

stabilized by three S–Au$_{surf}$ bonds plus the dispersive forces between its π-electronic system and the highly polarizable Au surface.[35] The computed binding energy of 182 kJ/mol is remarkably high. A dissociation of the TPB complex was found to be unfavorable on the Au(111), as discussed in the Supporting Information.

On the basis of the starting geometry, we have analyzed the interaction of the TPB with individual Au adatoms. The first species attached to the ligand hardly affects its binding configuration. The atom occupies a three-fold hollow site on the Au(111) that is adjacent to an S center in the TPB. The resulting S–Au$_{ad}$ distance amounts to 3 Å (Figure 7), which is considerably longer than the 2.5 Å bond length in a gas-phase TPB–Au complex. The larger binding distance reflects the competition between the S–Au$_{ad}$ and Au$_{ad}$–surface interaction that holds the adatom in place. Two other Au atoms can be coordinated in a similar way by the remaining S atoms of the TPB. However, the ligand is able to bind even three extra adatoms, which occupy Au(111) hollow sites below the upright standing phenyl rings. In this configuration, the bond length to the next S center increases to 4.0 Å and stabilization mainly arises from the interaction with a peripheral phenyl ring that slightly bends toward the adatom. A single flat-lying TPB ligand is therefore able to coordinate up to six Au adatoms. This surprisingly high capacity of thioethers to coordinate Au atoms is in agreement with earlier studies on short alkanethiolate chains.[22,36–38]

To connect the above-described binding geometries to ad-features observed in the experiment, we have simulated STM images with the Tersoff–Hamann approach.[28] The results did not reproduce the experimental data because of the overwhelming contrast induced by the upright standing phenyl rings (Figure 8a). Due to their large topographic height they imprint a pronounced three-fold symmetry onto the images that is independent of the actual number of adatoms attached to the ligands. This effect is an artifact of the Tersoff–Hamann model, which considers only the availability of electronic states in a certain energy window but not their suitability for electron

dx.doi.org/10.1021/ja300304s | J. Am. Chem. Soc. 2012, 134, 11161–11167

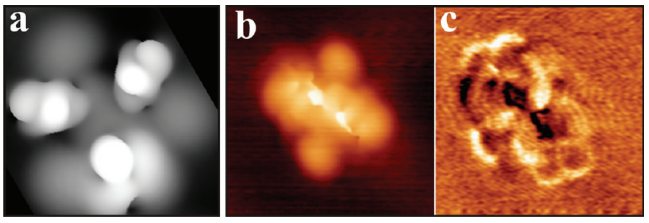

Figure 8. (a) Simulated STM images of a complete TPB molecule with four Au atoms attached. The simulation is artificially governed by the three upright-standing phenyl rings that are not observed in STM. Only at extremely short tip−sample distances, those units appear as fuzzy regions in the image, here shown for a dimer complex in the topographic (b) and the conductance channel (c) (30 × 30 Å^2, 25 mV). To remove such artifacts in the simulations, we have replaced the upright phenyls with hydrogen atoms.

transport. In contrast, STM is a transport experiment that measures the flux of electrons between tip and sample. Although the upright standing phenyl rings possess orbitals that might act as intermediate states for tunneling, they are unsuitable for electron transport due to a negligible overlap with the substrate electronic states. Consequently, the upright phenyl rings do not show up in experimental images taken at usual set-point parameters. Only at extremely short tip−sample distances, they leave observable traces in the STM images, as frequent collisions between tip and protruding molecular units induce heavy fluctuations on the tunnel current (Figure 8b,c).[39] Experimental and simulated STM data can however be reconciled if the upright phenyl rings are replaced by H atoms in the calculations (see Supporting Information for details). The resulting simulations perfectly reproduce the experimental data that have been obtained at low-temperature Au deposition onto a TPB-covered surface (compare Figures 5 and 7b). Apparently, a binding geometry in which the flat-lying central benzene is surrounded by up to six Au atoms is only realized at preparation temperatures below 100 K. The room-temperature complexes with their distinct dimer structure, on the other hand, seem to follow another building principle.

The main difference between low- and high-temperature TPB complexes is their apparent height in the STM, which amounts to 1.5 and 2.6 Å in the two cases. This suggests a larger interface distance between the room-temperature TPB and the gold surface. Moreover the spatial extension of the dimers (25 Å) is not compatible with a single TPB molecule anymore, which is only 10 Å in size. However, aggregation of two TPB monomers plus a few Au atoms could explain the observed features. Based on these considerations, we have developed thermodynamically stable dimer complexes at the PBE+D level. Two structures were identified, both of them being composed of two ligands connected via several bridging Au atoms (Figure 9). In the first conformer, the intermolecular interaction is mediated by four atoms occupying neighboring fcc and hcp binding sites in the Au(111) surface. The length of the bridging Au chain amounts to 7 Å, which is in good agreement with the short axis of the smaller dimer shown in Figure 4b. The long axis is defined by two additional adatoms that are attached to the outer S centers of the dimer and 18 Å apart. The second conformer deviates from the first one by the length of the central atom chain, which now comprises four Au atoms in fcc sites and is 9 Å long. This configuration can be reconciled with the long dimer structure in the experiment (Figure 4c). Similar to the short TPB dimer, also the long one

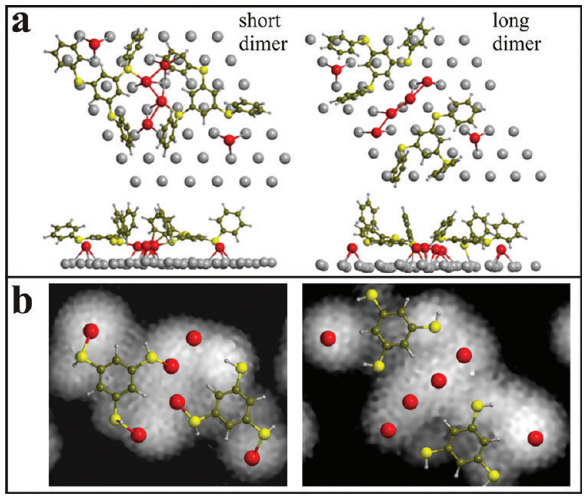

Figure 9. (a) Optimized structure of a TPB dimer complex in the short and long configuration on Au(111). (b) Simulated STM images with the respective ball models overlaid. The upright phenyl rings have been replaced with hydrogen. The images were obtained at an iso-density level of 0.0001 |e|/Å^3. The resulting configurations correspond to ad-features observed upon room-temperature deposition of TPB (Figure 4).

is able to trap two additional adatoms with its terminal S centers. Interestingly, dimerization always requires two Au-atom pairs in order to mediate the interaction between the two molecules. This can be explained with the steric repulsion exerted by the upright phenyl rings that inhibits the interconnection of two ligands via a single Au adatom. In contrast, the S-Au$_{ad}$-Au$_{ad}$-S units are flexible enough to mediate the bonding between two TPB molecules in a slightly staggered configuration.

The dimer models are in good agreement with the room-temperature complexes observed in STM. Their characteristic cross-like shape reflects the spatial arrangement of the Au atoms inside the metal−organic complexes. Whereas the Au pairs bridging the two TPBs generate the two bright protrusions in the center, the single atoms at the terminal sulfurs appear darker (Figure 4). We note that single Au adatoms and dimers on bare Au(111) display the same height difference, suggesting that the STM contrast is dominated by the gold and not by the molecular electronic states, which indeed feature a HOMO−LUMO gap of around 4 eV. Also the manipulation experiments confirm our structure model (Figure 6). Applying a controlled bias pulse breaks the compound into six identical protrusions, reflecting the six adatoms that have been trapped in the dimer. We suspect that the ligands themselves are removed from the surface during manipulation.

The results presented so far unambiguously demonstrate the ability of the TPB molecules to trap Au adatoms, which either originate from the Au(111) lattice gas or have been co-deposited onto the surface. This conclusion is in perfect agreement with the widely accepted picture that thiolates bind to the Au(111) by means of single adatoms.[29,30,36] The ligands therefore fulfill a first requirement to serve as potential redispersion agent on a catalyst surface.

3.4. Energetics of Au Complexation by the TPB Ligands. To get a better idea on the interaction strength between the ligand molecules and the Au atoms, typical Au complexation processes have been simulated on the basis of the most stable monomer and dimer structures.[17] DFT calculations

dx.doi.org/10.1021/ja300304s | J. Am. Chem. Soc. 2012, 134, 11161−11167

revealed that a single TPB monomer is able to coordinate up to six Au atoms on the Au(111) surface, as the following reaction is exothermic for $N \leq 6$:

$$\mathrm{TPB/Au(111)} + N[\mathrm{Au_1/Au(111)}] \rightarrow \mathrm{TPB{-}Au_N/Au(111)} + N\mathrm{Au(111)}$$

The reaction energy varies between −90 and −18 kJ/mol for N = 1−6 Au atoms attached to the ligand. The decline reflects the more and more unfavorable binding configuration of the adatoms at higher load. Also the energy for dissolving an Au_n cluster by a TPB monomer is negative for $N \leq 4$:

$$\mathrm{TPB/Au(111)} + \mathrm{Au_N/Au(111)} \rightarrow \mathrm{TPB{-}Au_N/Au(111)}$$

This implies that one ligand may disrupt an Au dimer, trimer, or tetramer cluster. Finally, extracting a single atom from an Au_N cluster via attachment to a TPB molecule has found to be favorable, as suggested by the exothermic character of the following reaction:

$$\mathrm{TPB/Au(111)} + \mathrm{Au_N/Au(111)} \rightarrow \mathrm{TPB{-}Au_1/Au(111)} + \mathrm{Au_{N-1}/Au(111)}$$

For $N > 2$, i.e., beyond the Au dimer, the associated energy is of the order of −50 kJ/mol.[17]

Also the attachment of six adatoms to a TPB dimer has found to be exothermic, yielding an excess energy of −33 and −39 kJ/mol for the long and short conformer, respectively. Values for lower loads (N = 1−5) cannot be determined as the dimer configuration is stable only in the presence of all six atoms. Moreover, a TPB dimer is able to break apart an Au_6 cluster, as the corresponding energy is negative for the short (−17 kJ/mol) and long conformer (−50 kJ/mol). In general, the average attachment energy per ligand is higher for the flat-lying monomer compared to the up-lifted dimer structure. However, this advantage is lost as two monomers spontaneously transform into a dimer at ∼100 K, a process that is described by the following reaction:

$$2[\mathrm{TPB{-}Au_3/Au(111)}] \rightarrow \mathrm{TPB_2{-}Au_6/Au(111)} + \mathrm{Au(111)}$$

In agreement with experiment, dimerization is exothermic for two monomers being loaded with three adatoms and yields an energy gain of −11 and −44 kJ/mol for the short and long conformer, respectively. The reaction becomes even more exothermic for TPB monomers loaded with six Au atoms, as the excess atoms freed upon dimerization can reaggregate into an Au_6 cluster.

All exchange reactions discussed here indicate that disruption of small Au clusters and binding of the released atoms to a TPB ligand is energetically favorable at certain conditions. However, our considerations provide information only on the energy balance of such virtual reactions, but not on possible reaction pathways or kinetic barriers. Nonetheless, we suspect that metal redisperison via TPB molecules might be feasible.

3.5. TPB Interactions with Au Particle Ensembles Grown on Thin Alumina Films. In order to explore the impact of the TPB molecules on a system that is closer to a real catalyst than Au(111), we have prepared an Au particle ensemble on an oxide thin film and exposed it to the ligand molecules (Figure 10a). For this purpose, an ultrathin alumina film was grown by oxidizing a NiAl(110) single crystal and annealing it to 1050 K. The resulting film is crystalline and atomically flat and consists of two Al−O bilayers. Details of its atomic structure and electronic nature can be found in the literature.[40,41] The Au ad-particles were produced by dosing ∼1.5 ML Au from a Mo crucible onto the surface at room temperature. The particles have been stabilized and homogenized with respect to their geometry by annealing the sample to 600 K for 10 min. The final ensemble properties are given by a particle density of $\sim 3 \times 10^{12}$ cm^{-1} and a mean particle diameter of 40 ± 10 Å.

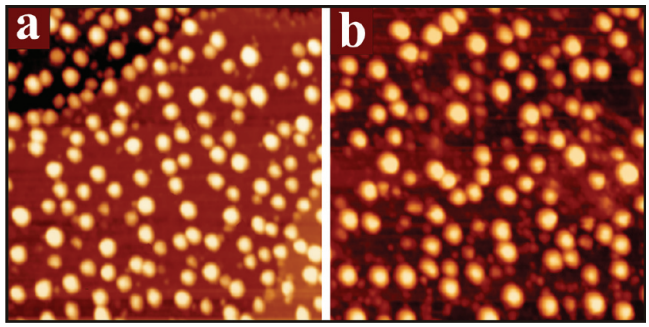

Figure 10. STM topographic images of Au particle ensemble grown on a thin alumina/NiAl(110) film (70 × 70 $Å^2$, −1.5 V). Whereas image a shows the pristine surface, image b was obtained after dosing 100 L of TPB at 400 K. Note the large number of small ad-features between the Au deposits, assigned to TPB−Au complexes.

To stimulate redispersion of the gold, we have exposed the sample to a flux of TPB molecules at 400 K for ∼10 min (local TPB pressure 1×10^{-7} mbar). Although the initial particle geometry did not change considerably, numerous new aggregates were detected in the STM images after exposure (Figure 10b). The new species are 15 Å in size and assigned to TPB molecules that have trapped mobile Au atoms diffusing between the larger deposits. We are unable to provide insight into the internal structure of the complexes at this point, due to difficulties to scan the insulating oxide at low bias. However, in control experiments performed without TPB exposure, hardly any new ad-features were detected, and only the density of the original Au deposits decreased slightly due to Ostwald ripening. On the other hand, the new ad-features were found to completely fill up the oxide surface upon exposure to a 10 000 times higher TPB flux, indicating a substantial material transport from the Au deposits to the bare oxide. An even more drastic effect on the particle size distribution is expected when dosing the molecules at catalytically relevant pressures and temperatures; however the realization of such experiments is beyond the scope of this work.

4. CONCLUSIONS

High purity thiophenyl derivatives have been successfully synthesized and investigated with respect to their adsorption behavior on Au(111) with STM and DFT. Our study revealed an effective stabilization of mobile atoms from the Au(111) lattice gas by incorporating them into various metal−organic complexes. The most stable isomer was found to comprise two TPB molecules tied together by an Au_4 chain, which gives rise to characteristic cross-like features in the STM. At low temperature, even single ligand molecules were found to trap up to six metal adatoms. The stabilization of mobile Au species via complexation with the TPB was observed even on an oxide

dx.doi.org/10.1021/ja300304s | J. Am. Chem. Soc. 2012, 134, 11161−11167

surface covered with Au deposits, where new ultrasmall aggregates have been detected after ligand exposure.

Our results provide evidence that TPB molecules are able to influence diffusion processes on oxide surfaces and therewith a decisive requirement for Ostwald ripening to occur. Moreover, the formation of stable metal−organic complexes may be considered as a first step to trigger the formation of new aggregates, causing the particle-size distribution to shift to lower values. In future experiments, we need to explore how the ligand molecules can be removed from the surface again in order to avoid poisoning effect by carbon residues. Possible methods include photochemical bleaching or ozone etching. Only after complete ligand removal, the original chemical state of the catalyst is recovered and the redispersion cycle is closed.

■ ASSOCIATED CONTENT

Supporting Information

Infrared absorption−reflection data of TPB on Au(111), dissociation energies for the optimized molecular structures, and details of the STM imaging process. This material is available free of charge via the Internet at http://pubs.acs.org.

■ AUTHOR INFORMATION

Corresponding Author

nilius@fhi-berlin.mpg.de; blechert@chem.tu-berlin.de; js@chemie.hu-berlin.de

Notes

The authors declare no competing financial interest.

■ ACKNOWLEDGMENTS

This work has been supported by the DFG through the "Cluster of Excellence UNICAT". We acknowledge support from the Norddeutscher Verbund für Hoch- und Höchstleistungsrechnen.

■ REFERENCES

(1) Ertl, G.; Knözinger, H.; Schueth, F.; Weitkamp, J. *Handbook of heterogeneous catalysis*, 2nd ed.; Wiley-VCH: Weinheim, 2008.

(2) (a) Haruta, M.; Yamada, N.; Kobayashi, T.; Iijima, S. *J. Catal.* **1989**, *115*, 301. (b) Haruta, M. *Cat. Tech* **2002**, *6*, 102.

(3) Todd, P.; St. Clair, D.; Goodman, D. W. *Top. Catal* **2000**, *13*, 5.

(4) Hayden, B. E.; Pletcher, D.; Rendall, M. E.; Suchsland, J. P. *J. Phys. Chem. C* **2007**, *111*, 17044.

(5) Risse, T.; Shaikhutdinov, S.; Nilius, N.; Sterrer, M.; Freund, H.-J. *Acc. Chem. Res.* **2008**, *41*, 949.

(6) Lin, X.; Nilius, N.; Freund, H.-J.; Walter, M.; Frondelius, P.; Honkala, K.; Häkkinen, H. *Phys. Rev. Lett.* **2009**, *102*, 206801.

(7) Molina, L. M.; Hammer, B. *Appl. Catal., A* **2005**, *291*, 21−31.

(8) Yoon, B.; Häkkinen, H.; Landman, U.; Wörz, A. S.; Antonietti, J.; Abbet, S.; Judai, J.; Heiz, U. *Science* **2005**, *307*, 403.

(9) Campbell, C. T. *Surf. Sci. Rep.* **1997**, *27*, 1.

(10) Narayanan, R.; El-Sayed, M.-A. *J. Am. Chem. Soc.* **2003**, *125*, 8340.

(11) Voorhees, P. W. *J. Stat. Phys.* **1985**, *38*, 231.

(12) Starr, D. E.; Shaikhutdinov, S. K.; Freund, H. J. *Top. Catal.* **2005**, *36*, 33.

(13) Monzon, A.; Garetto, T. F.; Borgna, A. *Appl. Catal., A* **2003**, *248*, 279−289.

(14) Bernal, S.; Botana, F. J.; Calvino, J. J.; Cifredo, G. A.; Perezomil, J. A. *Catal. Today* **1995**, *23*, 219−250.

(15) Fung, S. C. *Catal. Today* **1999**, *53*, 325−338.

(16) Chen, M. S.; Goodman, D. W. *Chem. Soc. Rev.* **2008**, *37*, 1860−1870.

(17) Tosoni, S.; Boese, D. A.; Sauer, J *J. Phys. Chem. C* **2011**, *115*, 24871−24879.

(18) (a) Barth, J. V.; Costantini, G.; Kern, K. *Nature* **2005**, *437*, 671. (b) Dmitriev, A.; Spillmann, H.; Lin, N.; Barth, J. V.; Kern, K. *Angew. Chem., Int. Ed.* **2003**, *42*, 2670.

(19) James, S. L. *Chem. Soc. Rev.* **2003**, *32*, 276−288.

(20) Stepanow, S.; Lin, N.; Payer, D.; Schlickum, U.; Klappenberger, F.; Zoppellaro, G.; Ruben, M.; Brune, H.; Barth, J. V.; Kern, K. *Angew. Chem., Int. Ed.* **2007**, *46*, 710−713.

(21) Zacher, D.; Shekhah, O.; Wöll, C.; Fischer, R. A. *Chem. Soc. Rev.* **2009**, *38*, 1418−1429.

(22) Poirier, G. E.; Pylant, E. D. *Science* **1996**, *272*, 1145−1148.

(23) Rust, H.-P.; Buisset, J.; Schweizer, E. K.; Cramer, L. *Rev. Sci. Instrum.* **1997**, *68*, 129.

(24) (a) Perdew, J. P.; Chevary, J. A.; Vosko, S. H.; Jackson, K.A..; Pederson, M. R.; Singh, D. J.; Fiolhais, C. *Phys. Rev. B* **1992**, *46*, 6671. (b) Kresse, G.; Furthmüller, J. *Comput. Mater. Sci.* **1996**, *6*, 15.

(25) (a) Blöchl, P. E. *Phys. Rev. B* **1994**, *50*, 17953−17959. (b) Kresse, G.; Joubert, J. *Phys. Rev. B* **1999**, *59*, 1758−1775.

(26) (a) Grimme, S. *J. Chem. Phys.* **2006**, *124*, 034108. (b) Kerber, T.; Sierka, M.; Sauer, J. *J. Comput. Chem.* **2008**, *29*, 2088.

(27) Tonigold, K.; Gross, A. *J. Chem. Phys.* **2010**, *132*, 224701.

(28) Tersoff, J.; Hamann, D. R. *Phys.Rev. B* **1985**, *31*, 805.

(29) Molina, L. M.; Hammer, B. *Chem. Phys. Lett.* **2002**, *360*, 264−271.

(30) Pyykkö, P. *Chem. Soc. Rev.* **2008**, *37*, 1967−1997.

(31) (a) Reifschneider, W. US Patent, 3102916, 19630903, 1963. (b) Adams, R.; Reifschneider, W.; Ferreti, A. *Org. Synth.* **1973**, *5*, 107.

(32) Wan, L. J.; Terashima, M.; Noda, H.; Osawa, M. *J. Phys. Chem. B* **2000**, *104*, 3563−3569.

(33) Syomin, D.; Kim, J.; Koel, B. E.; Ellison, G. B. *J. Chem. Phys. B* **2001**, *105*, 8387−8394.

(34) Rienks, E. D. L.; Nilius, N.; Rust, H.-P.; Freund, H.-J. *Phys. Rev. B* **2005**, *71*, 241404.

(35) (a) Baber, A. E.; Tierney, H. L.; Sykes, E. C. H. *ACS Nano* **2008**, *2*, 2385−2391. (b) Tierney, H. L.; Baber, A. E.; Sykes, E. C. H.; Akimov, A; Kolomeisky, A. B. *J. Phys. Chem. C* **2009**, *113*, 10913−10920.

(36) (a) Maksymovych, P.; Sorescu, D. C.; Yates, J. T. *Phys. Rev. Lett.* **2006**, *97*, 146103. (b) Maksymovych, P.; Yates, J. T. *J. Am. Chem. Soc.* **2008**, *130*, 7518.

(37) (a) Grönbeck, H.; Häkkinen, H.; Whetten, R. L. *J. Phys. Chem. C* **2008**, *112*, 15940. (b) Mazzarello, R.; Cossaro, A.; Verdini, A.; Rousseau, R.; Casalis, L.; Danisman, M. F.; Floreano, L.; Scandolo, S.; Morgante, A.; Scoles, G. *Phys. Rev. Lett.* **2007**, *98*, 016102.

(38) Weidner, T.; Ballav, N.; Siemeling, U.; Troegel, D.; Walter, T.; Tacke, R.; Castner, D. G.; Zharnikov, M. *J. Phys. Chem. C* **2009**, *113*, 19609−19617.

(39) Another reason for the invisibility of upright phenyl rings might be their quick motion below the tip. Using Hessian harmonic frequency calculations, we have identified the torsion of those groups to be the lowest vibrational excitation (1−7 meV) that can be excited by inelastic electron tunneling even at 5 K. This motion leads to a blurred topographic signature of the peripheral rings and renders their identification difficult

(40) (a) Jäger, R. M.; Kuhlenbeck, H.; Freund, H. J.; Wuttig, M.; Hoffmann, W.; Franchy, R.; Ibach, H. *Surf. Sci.* **1991**, *259*, 235−252. (b) Kulawik, M.; Nilius, N.; Rust, H.-P.; Freund, H.-J. *Phys. Rev. Lett.* **2003**, *91*, 256101.

(41) Kresse, G.; Schmid, M.; Napetschnig, E.; Shishkin, M.; Köhler, L.; Varga, P. *Science* **2005**, *308*, 1440−1442.